AFRL-ML-WP-TP-2007-401

FINITE ELEMENT ANALYSIS OF MULTILAYERED AND FUNCTIONALLY GRADIENT TRIBOLOGICAL COATINGS WITH MEASURED MATERIAL PROPERTIES (PREPRINT)

Young Sup Kang, Shashi K. Sharma, Jeffrey H. Sanders, and Andrey A. Voevodin

NOVEMBER 2006

Approved for public release; distribution unlimited.

**MATERIALS AND MANUFACTURING DIRECTORATE
AIR FORCE RESEARCH LABORATORY
AIR FORCE MATERIEL COMMAND
WRIGHT-PATTERSON AIR FORCE BASE, OH 45433-7750**

NOTICE AND SIGNATURE PAGE

AFRL-ML-WP-TP-2007-401 HAS BEEN REVIEWED AND IS APPROVED FOR PUBLICATION IN ACCORDANCE WITH ASSIGNED DISTRIBUTION STATEMENT.

*//Signature//   //Signature//

ANDREY A. VOEVODIN, Program Manager   JEFFREY H. SANDERS, Chief
Nonstructural Materials Branch   Nonstructural Materials Branch
Nonmetallic Materials Division   Nonmetallic Materials Division

//Signature//

SHASHI K. SHARMA, Acting Deputy Chief
Nonmetallic Materials Division
Materials and Manufacturing Directorate

REPORT DOCUMENTATION PAGE

1. REPORT DATE *(DD-MM-YY)*	2. REPORT TYPE	3. DATES COVERED *(From - To)*
November 2006	Journal Article Preprint	

4. TITLE AND SUBTITLE	5a. CONTRACT NUMBER
FINITE ELEMENT ANALYSIS OF MULTILAYERED AND FUNCTIONALLY GRADIENT TRIBOLOGICAL COATINGS WITH MEASURED MATERIAL PROPERTIES (PREPRINT)	F33615-03-D-5801
	5b. GRANT NUMBER
	5c. PROGRAM ELEMENT NUMBER 62102F

6. AUTHOR(S)	5d. PROJECT NUMBER 4349
Young Sup Kang (Universal Technology Corporation) Shashi K. Sharma, Jeffrey H. Sanders, and Andrey A. Voevodin (AFRL/MLBT)	5e. TASK NUMBER LO
	5f. WORK UNIT NUMBER VT

7. PERFORMING ORGANIZATION NAME(S) AND ADDRESS(ES)		8. PERFORMING ORGANIZATION REPORT NUMBER
Universal Technology Corporation 1270 N. Fairfield Road Dayton, OH 45432	Nonstructural Materials Branch (AFRL/MLBT) Nonmetallic Materials Division Materials and Manufacturing Directorate Air Force Research Laboratory, Air Force Materiel Command Wright-Patterson Air Force Base, OH 45433-7750	

9. SPONSORING/MONITORING AGENCY NAME(S) AND ADDRESS(ES)	10. SPONSORING/MONITORING AGENCY ACRONYM(S) AFRL-ML-WP
Materials and Manufacturing Directorate Air Force Research Laboratory Air Force Materiel Command Wright-Patterson AFB, OH 45433-7750	11. SPONSORING/MONITORING AGENCY REPORT NUMBER(S) AFRL-ML-WP-TP-2007-401

12. DISTRIBUTION/AVAILABILITY STATEMENT

13. SUPPLEMENTARY NOTES

14. ABSTRACT
Proper design of functionally gradient (FG) coatings requires a thorough understanding of layer architecture, chemistry and mechanical properties. An elastic-plastic model has been developed to study the stress distribution in multilayered FG coatings using finite element method to achieve optimum design architecture for high wear resistance and low friction. $Ti_{1-x}C_x$ $(0 \leq x \leq 1)$ gradient coatings with diamond like carbon (DLC) coating on 440C stainless steel substrate were assumed as a series of perfectly bonded layers with unique material properties and layer thickness. In order to model the elastic-plastic behavior of these coatings accurately, nano-indentation experiments using a nano-indenter were performed to measure material properties of each $Ti_{1-x}C_x$ gradient coating block. Using measured material properties, the numerical elastic-plastic model was used to examine the threshold of plasticity and plastic deformation zone inside the multilayered coatings and substrate and at the multilayered interfaces.

15. SUBJECT TERMS
Functionally gradient (FG) coatings; elastic-plastic model; $Ti_{1-x}C_x$ gradient coating; nano-indentation

16. SECURITY CLASSIFICATION OF:			17. LIMITATION OF ABSTRACT:	18. NUMBER OF PAGES	19a. NAME OF RESPONSIBLE PERSON (Monitor)
a. REPORT Unclassified	b. ABSTRACT Unclassified	c. THIS PAGE Unclassified	SAR	36	Andrey A. Voevodin 19b. TELEPHONE NUMBER *(Include Area Code)* N/A

Abstract

Proper design of functionally gradient (FG) coatings requires a thorough understanding of layer architecture, chemistry and mechanical properties. An elastic-plastic model has been developed to study the stress distribution in multilayered FG coatings using finite element method to achieve optimum design architecture for high wear resistance and low friction. $Ti_{1-x}C_x$ ($0 \leq x \leq 1$) gradient coatings with diamond like carbon (DLC) coating on 440C stainless steel substrate were assumed as a series of perfectly bonded layers with unique material properties and layer thickness. In order to model the elastic-plastic behavior of these coatings accurately, nanoindentation experiments using a nano indenter were performed to measure material properties of each $Ti_{1-x}C_x$ gradient coating block. Using measured material properties, the numerical elastic-plastic model was used to examine the threshold of plasticity and plastic deformation zone inside the multilayered coatings and substrate and at the multilayered interfaces.

Introduction

Wear protective coatings have been developed to protect the contacting surfaces from friction and wear. Depending on the coating applications, the design, composition, and thickness of the wear protective coatings vary. Nevertheless, the main functional factors such as high hardness and low friction for wear protective coatings remain the same. One of the widely used wear protective coatings is the diamond like carbon (DLC) coating deposited at low temperatures because it has the high hardness and low friction characteristics. Although there are many superior advantages for DLC coatings, their applications are limited to the contact pressure, 1 GPa, due to the weak adhesion between the DLC coating and the softer substrate. Lyubimov et al. (1992) found that interfaces between layers are the prime locations for the film failure, e.g. by an interface crack growth, because of the considerable mechanical property differences at the interfaces. Also, due to the intrinsic stresses created by the deposition process, the thickness of the DLC coating is limited to 0.5 µm (Voevodin et al., 1997b). To eliminate the usage limitations of the DLC coatings, a multilayer design was proposed. In order to increase the adhesion between the DLC coating and the substrate, the bond layer such as α-Ti layer was used. Also, to provide the load support mechanism for DLC layers, functionally gradient (FG) architectures have been developed. Therefore, the FG Ti/TiC/DLC multilayered coating system has been developed extensively for the high load and wear resistant applications because of the unique combination of high hardness, load support, and low friction (Voevodin et al., 1995, 1997a, 1997b). Lyubimov et al. (1992) concluded that the optimal choice of thickness, combination, and deposition conditions of layers should consider their stress state to prevent failure of a multilayer coating. Therefore, in order to develop the optimal FG Ti/TiC/DLC multilayered coating system design, the stress distribution and elastic-plastic deformation of the coating system should be investigated.

In addition, to develop the numerical models accurately, the material properties such as hardness, modulus of elasticity, and yield strength need to be measured and calculated for each thin coating. Due to the thickness of the thin coatings, conventional tensile test cannot be performed to generate the stress strain relationship curve for each coating material. One of the most widely used methods to measure the material properties for thin coatings is the nanoindentation developed for characterizing thin coatings and layers mechanically because nanoindentation of thin coatings provides a relatively simple approach to quantify the mechanical properties of thin coatings. Due to the thickness of the thin coatings, only shallow indentation depth is allowed to extract the measurement data from the thin coating systems. From the nanoindentation of coating systems, the load vs. indentation depth curves are obtained and analyzed to determine properties such as modulus of elasticity and hardness as well as to study the elastic-plastic deformation mechanisms. Nanoindentation has become widely used for the characterization of coated systems over the past three decades. Doerner and Nix (1986) developed a method for interpreting hardness and Young's modulus from the data obtained from depth-sensing indentation instruments. Later, Pharr and Oliver (1992) proposed the improved nanoindentation technique and conducted the experimental measurements of thin film mechanical properties such as hardness and modulus of elasticity, that is, properties are derived from measurements of load, displacement, and time. Page and Hainsworth

(1993) reviewed and summarized the abilities and limitations of nanoindentation techniques to characterize the mechanical properties of thin coatings. They considered these nanoindention systems as ultimate mechanical property microprobes that characterize thin coatings. Nanoindentation technique has been used by Voevodin et al. (1995) to evaluate the mechanical properties of diamond-like carbon (DLC) coatings prepared by pulsed laser deposition. There have been numerous analytical and finite element models developed for the nanoindentation of thin coatings. (Knapp et al., 1996, 1997,1999, Bouzakis et al., 2001, Chudoba et al., 2002). They also conducted nanoindentation experiements for various types of coated systems and developed the procedures for obtaining the mechanical properties of thin coatings based on finite-element modeling of nanoindentation. They emphasized the situation when substrate effects for thin coating mechanical properties measurement are dominant, that is, the thin hard coatings over softer substrates.

In this present work, the elastic plastic finite element analysis model using measured material properties has been developed due to the nonlinear nature of the coating system. The FEA model has been used to determine the stress distribution in the FG Ti/TiC/DLC multilayered tribological coating system and examine the elastic plastic deformation of the coating systems during indentation. Nanoindentation experiments were conducted to measure the material properties such as hardness and modulus of elasticity for each coating material. In addition, nanoindentation FEA simulation was performed to calculate the yield strength of each coating material. The ultimate goal of this study is to develop optimized FG multilayered coatings for high adhesion and scratch resistant applications.

Functionally Gradient (FG) Multilayered Tribological Coating
Voevodin et al. (1997b) illustrated the need for the functionally gradient (FG) multilayered tribological coatings in heavily loaded contact applications. Figure 1 shows the FG Ti/TiC/DLC coating system developed by Voevodin et al. (1997b). Instead of having diamond like carbon (DLC) coating on the top of the substrate, there is Ti/TiC coating system that has gradual Ti and C composition changes to improve the load support and adhesion between the DLC coating and the substrate.

Nanoindentation
To measure the material properties such as hardness and modulus of elasticity for FG Ti/TiC/DLC coating system, a MTS nano indenter® XP was used for the experiment under the carefully controlled environment. Figure 2 depicts the schematic of nanoindentation for multilayered semi-infinite medium with a spherical indenter tip. The spherical indenter tip is loaded vertically during nanoindentation. It is assumed that gradient coatings have a series of perfectly bonded block layers with unique material properties and layer thickness. However, the gradient coatings don't have distinct layers in reality. They normally have continuous gradual change of Ti and C composition. It is also assumed that there is no interfacial stress generated by the deposition process at the interfaces. In order to develop an accurate nanoindentation model for the FG Ti/TiC/DLC coating system, material property measurements for the inputs to the FEA model are required. It is difficult to measure the material properties for each distinct layer from the FG multilayered coating system because the material property measurements for thin coatings require very sophisticated instruments due to the

3

magnitude of coating thickness. Nano indenters with nano-Newton resolution in loading and nano-meter resolution in displacement allow very accurate measurements of the load-displacement curve for the thin coatings. Figure 3 demonstrates a portion of two dimensional axi-symmetric FEA model of the nanoindentation simulation using a conical indenter tip for coating samples. This FEA model was used for various coating samples to calculate their yield strengths of thin coatings using measured hardness (H) and modulus of elasticity (E) data. Knapp et al. (1996) developed the two dimensional axi-symmetric FEA model with the shape of the conical indenter tip to verify that the conical tip with a certain angle has the same area versus depth relationship for the Berkovich indenter tip. A diamond Berkovich tip was used for the nanoindentation experiments to measure the hardness and modulus of elasticity of thin coatings. Since the hardness of thin coating materials are relatively high, the deformation of the diamond indenter tip is not avoidable. Therefore, the deformable indenter tip was used for the FEA model. Each coating sample consists of 1 μm thick coating and 440C stainless steel substrate. The area function for the Berkovich indenter tip was calibrated through a series of nanoindentation onto fused silica sample. Nanoindentation experiment was performed for the carefully prepared samples to minimize the measurement errors.

Figure 4 illustrates the general load vs. displacement curves generated by the nanoindentation experiments. The red dots show the typical load vs. displacement curve for elastic deformation. The reversible load vs. displacement curve was generated during loading and unloading when the nanoindentation causes the elastic deformation on the sample surface. The blue dots depict the typical load vs. displacement curve for elastic-plastic deformation. During loading, the indenter tip makes a permanent impression on the sample surface due to the plastic response of the sample. The load vs. displacement curve during loading provides the hardness information of the materials. During unloading, the load vs. displacement curve is controlled by the elastic response of the sample. The load vs. displacement curve during unloading provides the modulus of elasticity information of the materials.

Measurement and Modeling Procedure for Yield Strength

From the nanoindentation experiments, the hardness and modulus of elasticity for thin coating materials are measured. However, to develop the elastic-perfectly plastic FEA model for FG Ti/TiC/DLC coating system, the yield strengths of thin coating materials should be obtained. Although there are no measured yield strength results from nanoindentation experiments, by the aid of the numerical nanoindentation simulation using a FEA model, the yield strengths of thin coatings are able to be calculated. Therefore, interactive procedure between FEA model simulations and nanoindentation experiments is required to calculate the yield strengths of the thin coating materials. It is assumed that the plastic deformation of a coating is initiated when its von Mises stress generated inside the coating becomes greater than yield strength of the coating material.

Nano Indenter Yield Strength Calculation

The procedure to calculate yield strength of a coating material is the following. The measurement of TiC/DLC coating material properties such as hardness and modulus of elasticity was conducted using a MTS nano indenter with a Berkovich indenter tip. The measured modulus of elasticity of the coating material is used as an input to the FEA model for the nanoindentation simulation. Also, yield strength of the coating material

should be used as an input for the nanoindentation simulation. The initial yield strength of the coating material is guessed based on the measured hardness value of the material. This step requires an iterative procedure to obtain a best-fit load vs. displacement curve from the nanoindentation simulation by changing the yield strength input value for the simulation. Therefore, when the computational best-fit load vs. displacement curve matches the experimental averaged load vs. displacement curve closely, the guessed yield strength value is considered as the yield strength of the material. Yield strength of each sample is determined from the nanoindentation simulation.

To calibrate the indenter tip area function, a series of indentation was performed on fused silica (SiO_2) because SiO_2 is a standard material for nanoindentation. The indentation depth was limited to 100 nm because each TiC/DLC coating sample has 1 μm coating thickness. To avoid the substrate effect on the material property measurement of thin coating materials, 1/10 rule was applied. Twenty five indentation tests were performed on the SiO_2 with 100 nm indentation depth. The nanoindentation experiment results for SiO_2 are in shown Figures 5 (a) through 5 (d). Figure 5(a) depicts the hardness vs. displacement curves for SiO_2. The measured average value for the hardness of SiO_2 is 8.9 ± 0.4 GPa. Figure 5(b) demonstrates the modulus of elasticity vs. displacement curves for SiO_2. The measured average value for modulus of elasticity of SiO_2 is 72.3 ± 3.5 GPa. Hardness values were taken at the maximum penetration depths, and modulus were calculated from the upper unloading portions of the load-displacement curves (Voevodin et al.,1997b). Figure 5(c) illustrates the load vs. displacement curves of corresponding to the hardness and modulus of elasticity curves of SiO_2. During loading, SiO_2 deforms elastically and then yields. During unloading, the elastic deformation of SiO_2 is recovered while the plastic deformation remains as a permanent impression on the contact surface. The load vs. displacement curve comparison between the experimental results and FEA results on SiO_2 is shown in Figure 5(d). The yield strength value of SiO_2 was determined by FEA model nanoindentation simulation. Since the measured average modulus of elasticity of SiO_2 is 72.3 GPa from nanoindentation test, 72.3 GPa is used as an input value to FEA model simulation for SiO_2. Circles show the load vs. displacement curve using average nanoindentation experimental results. The best-fit solid line is obtained through the FEA nanoindentation model simulation. Y = 7.1 GPa and E = 72.3 GPa were used for the inputs to nanoindentation simulation because Y = 7.1 ± 0.3 GPa and E = 73 ± 0.5 GPa were found in the literature (Knapp et al., 1999). The results indicate that the best-fit load vs. displacement curve from FEA model simulation agrees well with the average load vs. displacement curve from the nanoindentation experiment.

Nanoindentation experiments were conducted for 440C stainless steel because 440C stainless steel is used for the substrate of all Ti/TiC/DLC coating samples. Figure 6(a) shows the load vs. displacement curves for 440C stainless steel during loading and unloading stages of nanoindentation. Due to the surface roughness of 440C stainless steel, experimental curves are scattered. Because of the nature of the 440C stainless steel, higher load, ~1.8 mN, was required to make indentations upto 100 nm in depth than SiO_2. Also, the slope of the load vs. displacement curves during unloading for 440C stainless steel is steeper than the slope of the load vs. displacement curves during unloading for SiO_2. Figure 6(b) displays the comparison of load vs. displacement curves between the average experimental results and the best-fit FEA results. The average

experimental load vs. displacement curve matches the best-fit computational load vs. displacement curve when Y = 4.0 GPa and E = 220 GPa are used.

Nanoindentation for Ti/TiC/DLC Coating Material Properties

TiC/DLC coating samples were prepared by a hybrid of magnetron sputtering and pulsed laser deposition. Crystalline α-Ti, TiC and amorphous DLC films were formed at 100 °C substrate temperature by varying film composition. X-ray photoelectron spectroscopy (XPS) was performed on the coatings for the characterization (Voevodin et al., 1995). Figure 7 shows the schematic of nanoindentation on coating sample to measure the material properties. Vertical displacement of the indenter tip is applied to the sample during the nanoindentation. The nanoindentation process was simulated by moving the indenter tip vertically with controlled displacement while calculating reaction force at the contacted area. 440C stainless steel is used as a substrate for all coating samples that have1 μm thick coating deposited. For the simulation, the coefficient of friction between the indenter tip and sample surface varies from 0.0 to 1.0. Table 1 consists of the measured material properties such as the modulus of elasticity and hardness for TiC/DLC coating samples. The results indicate that the hardness and modulus of elasticity changes drastically as Ti and C composition changes.

The experimental results for $Ti_{.53}C_{.47}$ coating from nanoindentation are shown in figure 8(a) through 8(d). The indentation depth to $Ti_{.53}C_{.47}$ coating sample is limited to 100 nm to avoid the substrate effect on measured material properties. The figure 8(a) shows scattered data for hardness vs. displacement curves because of the surface roughness effect on the measurement. The hardness increases as the nanoindentation depth increases for $Ti_{.53}C_{.47}$ coating. The average hardness of $Ti_{.53}C_{.47}$ coating from the nanoindentation experiments is 14.2 ± 1.8 GPa. The thick solid line represents the average hardness value of $Ti_{.53}C_{.47}$ coating along the indentation depth. The figure 8(b) depicts the modulus of elasticity vs displacement curves for $Ti_{.53}C_{.47}$ coating. The average modulus of elasticity of $Ti_{.53}C_{.47}$ coating is 231.1 ± 34.6 GPa. The thick solid line shows the average value of the modulus of elasticity for $Ti_{.53}C_{.47}$ coating along the indentation depth. The figure 8(c) illustrates the load vs. displacement curves for $Ti_{.53}C_{.47}$ coating from nanoindentation. Due to the roughness of surface, the data is scattered. The figure 8(d) shows the comparison of averaged experimental results and best-fit FEA results for $Ti_{.53}C_{.47}$ coating. The average load vs. displacement curve agrees well with best-fit load vs. displacement curve when Y = 10 GPa and E = 240 GPa are used for $Ti_{.53}C_{.47}$ coating nanoindentation simulation.

Figure 9 demonstrates the schematic of functionally gradient (FG) Ti/TiC/DLC coating system design with programmed variation of compositional and mechanical properties proposed by A. A. Voevodin (1997b). Each layer has its unique material properties and thickness. Hardness and modulus of elasticity of Ti/TiC/DLC coating system are measured from coating samples. 25 indentation locations per sample were averaged to obtain the statistical values. The yield strength for each coating material is calculated from FEA nanoindentation simulation using the measured hardness and modulus of elasticity. These are the values used for inputs to FEA model for this study. The material properties of each layer were linearly interpolated from the measured material properties data. To improve adhesion between the substrate and upper carbide layers, α-Ti is used as a bond layer.

Finite Element Model

Figures 10(a) and 10(b) show a schematic of nanoindentation on FG multilayered coating system with a spherical indenter tip and its corresponding finite element analysis model. Figure 10(b) depicts two dimensional axi-symmetric finite element analysis model used for the nanoindentation simulation that consists of loading stage and unloading stage. The radius of the diamond spherical indenter tip is 50 μm. Since the hardness of the DLC coating is as high as a diamond tip, the deformable diamond indenter tip is modeled for the nanoindentation simulation. Although the nominal dimension of the diamond indenter is 50 μm in radius, actual dimension of the diamond indenter is 46.95 μm in radius. ABAQUS/Standard was used to model the nanoindentation simulation on the multilayered FG Ti/TiC/DLC coating system. Due to the symmetry of the system, axi-symmetric model was developed to save the computational time. Also, the outer portion of semi-infinite medium used infinite elements to reduce the computing time. Two different types of elements, four-node bilinear, reduced integration with hourglass control element (CAX4R) and four-node linear one-way infinite element (CINAX4), were used.

Figure 11(a) shows the effect of multilayered FG Ti/TiC/DLC coating system on von Mises Stress distribution during the nanoindentation for indenter displacement, $\delta = 50$ nm and friction coefficient, $\mu = 0.0$. Figure 11(b) describes the schematic of FG multilayered coating system design used for this study. Figure 11(a) illustrates the von Mises stress profiles along the depth direction on the plane of symmetry at the center of contact. The dotted line represents the von Mises stress profile along the depth direction for the no coating system case. It shows the smooth variation of von Mises stress distribution along the depth direction. However, for the multilayered FG Ti/TiC/DLC coating system case, the discrete variation of von Mises stress profile at the interfaces exists. Inside the DLC coatings and FG TiC coatings, higher von Mises stresses were generated than the no coating case because of the higher moduli of elasticity for the DLC and TiC coating materials. If more distinct layers are used for the FG multilayered FEA model, the von Mises stress profile along the depth direction would be smoother, that is, $Ti_{.85}$, $Ti_{.75}$ and $Ti_{.65}$ are used.

Figures 12(a) through 12(d) show contour plots of the von Mises stress distributions for various indenter displacement depths, $\delta = 40$ nm, 80 nm, 120 nm, and 160 nm at the end of loading stage. The indenter displacement, $\delta = 40$ nm, generates the maximum Hertzian pressure, $P_h = 4.5$ GPa, at the contact for no coated elastic 440C stainless steel substrate. The indenter displacement, $\delta = 160$ nm, generates the maximum Hertzian pressure, $P_h = 9.0$ GPa, at the contact for no coated elastic 440C stainless substrate. Figure 12 (a) depicts the contour plot of von Mises stress distribution inside the FG multilayered coating system generated at the indenter displacement depth, $\delta = 40$ nm. The maximum von Mises stress, 3.64 GPa, occurs inside the FG TiC/DLC coating system. Figure 12 (b) displays the contour plot of von Mises stress distribution inside the FG multilayered coating system generated at the indenter displacement depth, $\delta = 80$ nm. The increase of the indenter displacement moves the maximum location of von Mises stress further below the contact surface. The wider contact width is generated due to the increase of the indenter displacement. The maximum von Mises stress, 4.89 GPa, occurs inside the FG TiC/DLC coating system. Figure 12 (c) demonstrates the contour plot of von Mises stress distribution inside FG multilayered coating system generated at the

7

indenter displacement depth, $\delta = 120$ nm. The maximum von Mises stress, 5.93 GPa, occurs inside the FG TiC/DLC coating system. Figure 12 (d) illustrates the contour plot of von Mises stress distribution inside FG multilayered coating system generated at the indenter displacement, $\delta = 160$ nm. Due to the magnitude of the yield strength of the 440C stainless steel substrate, plastic deformation of the substrate occurs. The maximum von Mises stress, 6.57 GPa, occurs inside the FG TiC/DLC coating system. Although the indenter displacement increases from $\delta = 40$ nm to $\delta = 160$ nm, the location of maximum von Mises stress generated at the contact remains inside DLC coatings. Also, as the indenter displacement increases, wider contact width and higher von Mises stress occur.

Figures 13(a) and 13(b) show the von Mises stress distribution for the contact condition, $\delta = 80$ nm and $\mu = 0.0$. Figure 13(a) depicts the von Mises stress distribution generated below the center of the contact along the depth direction on the plane of symmetry. Width-axis corresponds to the later surface distance. Depth = 0 representes the surface position. This indicates that the maximum von Mises stress occurs below the center of the contact inside DLC multilayered coating. Due to the distinct material properties for each coating layer, the von Mises stress distribution displays sharp stress changes at the interface. Figure 13 (b) illustrates the contour plot of von Mises stress distribution generated inside the multilayered FG Ti/TiC/DLC coating system.

Figures 14(a) through 14(d) show the effect of applied load on von Mises stress profiles at various indentation depths for the contact condition, $\mu = 0.0$. Figure 14 (a) depicts the von Mises stress profiles along the depth direction at the center of the contact for indentation depth, $\delta = 40$ nm, for both FG coated system and 440C stainless steel substrate. Without any coating on the 440C stainless steel substrate, the substrate has a smooth transition of von Mises stress profile along the depth direction with maximum 2.37 GPa located below the surface. However, the mutilayered FG Ti/TiC/DLC coating system has a drastic transition of von Mises stress profile along the depth direction. Especially maximum von Mises stress, 3.64 GPa, occurs at the TiC/DLC interface. Also, the minimum von Mises stress occurs at the bond layer with 1.46 GPa. Figure 14 (b) displays the von Mises stress profiles along the depth direction at the center of the contact for indentation depth, $\delta = 80$ nm. Without any coating on the 440C stainless steel substrate, the substrate has a smooth transition of von Mises stress profile along the depth direction with maximum 3.41 GPa below the contact surface. Due to the higher moduli of elasticity for TiC/DLC materials than 440C stainless steel, the von Mises stress generated inside the FG TiC/DLC coating system has much higher values than no coating case. The FG Ti/TiC/DLC coating system has a drastic transition of von Mises stress along the depth direction. Especially maximum von Mises stress, 4.89 GPa, occurs at the TiC/DLC interface. Also, the minimum von Mises stress occurs at the bond layer with 1.46 GPa. The stress generated at the bond layer interface does not exceed the yield strength of the α - Ti bond layer because of the elastic-perfectly plastic stress strain relationship assumption. As the indentation depth increases from $\delta = 40$ nm to Figure 14(c) shows the von Mises stress profiles along the depth direction at the center of the contact for indentation depth, $\delta = 120$ nm. Without the FG Ti/TiC/DLC multilayered coating system, the maximum von Mises stress, 4.00 GPa, occurs in the substrate and causes the plastic deformation inside the substrate. The FG TiC/DLC coating system has maximum von Mises stress, 5.93 GPa, at the DLC/TiC interface. At the α-Ti bond layer,

the von Mises stress was limited to 1.46 GPa because of the material properties of α-Ti layer. Figure 14(d) depicts the von Mises stress profiles along the depth direction at the center of the contact for indentation depth, $\delta = 160$ nm. Without the FG Ti/TiC/DLC multilayered coating, the maximum von Mises stress, 4.00 GPa, occurs in the substrate and causes the larger plastic deformation region inside the substrate. Although there is the FG Ti/TiC/DLC multilayered coating system, von Mises stress, 4.00 GPa, occurs inside the substrate and causes the plastic deformation region inside the substrate. The FG TiC/DLC coating system has maximum von Mises stress, 6.57 GPa, at the DLC/TiC interface. At the α-Ti bond layer, the von Mises stress was limited to 1.46 GPa because of the material properties of α-Ti layer. This indicates the effect of bond layer on the von Mises stress distribution, that is, there are significant changes of von Mises stress magnitude at the bond layer. Generally stress profile shape remains the same. However, the magnitude of von Mises stress increases as the indenter displacement increases.

Figures 15(a) through 15(d) show the contour plots of equivalent plastic strain distribution generated for FG multilayered coating system from the FEA model at various indentation depths. Figure 15 (a) illustrates contour plot of the equivalent plastic strain distribution generated inside the FG multilayered coating system at the end of loading stage. The figure indicates that the maximum equivalent plastic strain occurs at the α-Ti bond layer for the indenter displacement, $\delta = 40$ nm. The plastic strain was initiated at the α-Ti bond layer below the center of the contact with the maximum magnitude of 9.875×10^{-3}. Figure 15 (b) depicts the contour plot of equivalent plastic strain distribution generated inside the FG multilayered coating system for the indenter displacement, $\delta = 80$ nm. As the indenter displacement increases, the magnitude of the equivalent plastic strain is increased to 6.133×10^{-2} at the α-Ti bond layer. The location of the maximum equivalent plastic strain moves from the center of the contact to the edges of the contact. Figure 15 (c) demonstrates the contour plot of equivalent plastic strain distribution generated inside the FG multilayered coating system for the indenter displacement, $\delta = 120$ nm. As the indenter displacement increases, the magnitude of the equivalent plastic strain is increased to 1.611×10^{-1}. The location of the maximum equivalent plastic strain moves further from the axis of symmetry to the edges of the contact. Figure 15 (d) displays the contour plot of equivalent plastic strain distribution generated at the α-Ti bond layer for indenter displacement, $\delta = 160$ nm. As the indenter displacement increases, the magnitude of the equivalent plastic strain is increased to 2.598×10^{-1}. The location of the maximum equivalent plastic strain moves further from the center of the contact to the edges of the contact, i.e. the half contact width.

During the nanoindentation process, the multilayered FG Ti/TiC/DLC coating system still experiences the residual stress after the nano indenter tip is unloaded from the FG multilayered coating system. Figures 16(a) through 16(d) show the contour plots of residual von Mises stress distribution generated inside the multilayered FG Ti/TiC/DLC coating system obtained from the FEA model. As the indenter tip displacement increases, the multilayered FG Ti/TiC/DLC coating system shows the higher residual von Mises stresses generated inside the coating system. Figure 16 (a) depicts the contour plot of residual von Mises stress distribution after the indenter displacement, $\delta = 40$ nm, is applied and removed. The maximum residual von Mises stress, 8.178×10^8 Pa, is generated below the center of the contact. The location of the maximum residual stress is

at the α-Ti bond layer. Figure 16 (b) demonstrates the contour plot of residual von Mises stress distribution inside the Ti/TiC/DLC coating system after the indenter displacement, $\delta = 80$ nm, is applied and removed. The maximum residual von Mises stress generated below the contact is 1.460×10^9 Pa around the α-Ti bond layer. As the indentation depth increases, the larger region below the contact surface is influenced by the residual stress. Figure 16 (c) illustrates the contour plot of residual von Mises stress distribution inside the Ti/TiC/DLC coating system after the indenter displacement, $\delta = 120$ nm, is applied and removed. The maximum von Mises stress generated below the contact is 1.748×10^9 Pa around the α-Ti bond layer. Figure 16 (d) displays the contour plot of residual von Mises stress distribution inside the Ti/TiC/DLC coating system after the indenter displacement, $\delta = 160$ nm, is applied and removed. The maximum residual von Mises stress generated below the contact is 2.244×10^9 Pa around the α-Ti bond layer. Larger area of the coating system has the residual von Mises stress inside the Ti/TiC/DLC coating system after the indenter tip is load and removed from the contact for the indenter displacement, $\delta = 160$ nm.

Figure 17 shows the effect of coating system design on von Mises stress profiles inside the coating systems along the depth direction at the center of the contact on the plane of symmetry under the contact condition, $\delta = 200$ nm and $\mu = 0.0$. The dashdot line describes the von Mises stress profile variation from the substrate surface to 0.55×10^{-6} m below the substrate surface for the no coated substrate. The magnitude of the von Mises stress increases upto 4 GPa as the depth inside the substrate increases and remains constant due to the yield strength of 440C stainless steel. The dashed line represents the von Mises stress profile variation from the thin DLC coating surface to the substrate. The maximum von Mises stress, 5.67 GPa, occurs at the DLC coating and substrate interface. Also the maximum von Mises stress for the substrate is limited to 4.00 GPa. The dotted line reveals the stress profile variation across thickness of the thick DLC coating and substrate system. The maximum von Mises stress of 10.1 GPa occurs at the DLC coating and substrate interface. Drastic stress profile change occurs at the interface due to the different material properties.   The solid line shows the von Mises stress profile variation generated for the multilayered FG Ti/TiC/DLC coating system. The Ti/TiC/DLC coating system has relatively moderate stress variation across the thickness of the coating system compared to the thick monolayered DLC coating because of the gradually variation of material properties across the thickness of the coating system.

Summary
Nanoindentation technique has been used for the mechanical characterization of coating materials. The finite element analysis model extends the usage of nanoindentation technique to the calculation of material property such as yield strength from the experimental nanoindentation data such as hardness and modulus of elasticity. Therefore, nanoindentation simulation by the finite element analysis model has been performed to determine the yield strengths for the multilayered FG Ti/TiC/DLC coating materials based on the measured nanoindentation data. Using the measured and calculated material properties for the coating system, FEA model has been developed to investigate the stress distribution and elastic-plastic deformation generated inside the multilayered FG Ti/TiC/DLC coating system due to the nanoindentation.

10

The superiority of the multilayered FG Ti/TiC/DLC coating system at high load applications was shown and discussed. The multilayered FG Ti/TiC/DLC coating system improves the system integrity under the heavy loading condition. It significant reduces the magnitude of the maximum von Mises stress generated and the drastic stress profile variation across the thickness of the coating system than monolayered DLC coating system due to the moduli difference of the coating materials. Also, it improves the wear resistance and load support mechanism compared to both no coating system and monolayered DLC coating system. To improve the adhesion between the DLC/TiC coating system and substrate, the bond layer is used. However, due to the material properties of the bond layer materials, bond layers become the prime location of the plastic deformation under the severe high loading condition. The residual stress should be considered as a key design factor when the multilayered FG coating system is developed.

Reference

V.V. Lyubimov, A.A. Voevodin, S. E. Spassky and A. L. Yerokhin, 1992, "Stress analysis and failure possibility assessment of multilayer physically vapour deposited coatings", Thin Solid Films, 207, pp 117-125.

A. A. Voevodin, M. S. Donley, J. S. Zabinski, J. E. Bultman, 1995, "Mechanical and tribological properties of diamond-like carbon coatings prepared by pulsed laser deposition", Surface and Coating Technology, 76-77, pp 534-539.

A. A. Voevodin, M. A. Capano, S. J. P. Laube, M. S. Donley, and J. S. Zabinski, 1997a, "Design of a Ti/TiC/DLC functionally gradient coating based on studies of structural transitions in Ti-C thin films", Thin Solid Films, 298, pp 107-115.

A. A. Voevodin, S. D. Walck, J. S. Zabinski, 1997b, "Architecture of multilayer nanocomposite coatings with super-hard diamond-like carbon layers for wear protection at high contact loads", Wear, 203-204, pp 516-527.

M. F. Doerner and W. D. Nix, 1986, "A method for interpreting the data from depth-sensing indentation instruments", Material Research Society, 1(4) Jul/Aug, pp. 601-609.

G. M. Pharr, and W. C. Oliver, 1992, "Measurement of Thin Film Mechanical Properties Using Nanoindentation", MRS Bulletin, July, pp 28-33.

T.F. Page and S.V. Hainsworth, 1993, "Using Nanoindentation Techniques for the Characterization of Coated Systems: A Critique", Surface and Coatings Technology, 61, pp 201-208

J. A. Knapp, D. M. Follstaedt, and S. M. Myers, 1996, "Precipitate-hardened aluminum alloys formed using pulsed laser deposition", Journal of Applied Physics, Vol. 79, Num 2, pp 1116-1122.

J. A. Knapp, D. M. Follstaedt, J. C. Barbour, S. M. Myers, 1997, "Finite-element modeling of nanoindentation for determining the mechanical properties of implanted layers and thin films", Nuclear Instruments and Methods in Physics Research B, 127/128, pp 935-939.

J. A. Knapp, D. M. Follstaedt, S. M. Myers, J. C. Barbour, and T. A. Friedmann, 1999, "Finite-element modeling of nanoindentation", Journal of Applied Physics, Vol. 85, Num. 3, pp 1460-1474.

K. D. Bouzakis, N. Michailidis, G. Erkens, 2001, "Thin hard coating stress-strain curve determination through a FEM supported evaluation of nanoindentation test results," Surface and Coatings Technology, 142-144, pp. 102-109.

T. Chudoba, N. Schwarzer, F. Richter, 2002, "Steps towards a mechanical modeling of layered systems," Surface and Coatings Technology, 154, pp 140-151.

Samples	Material Properties
DLC at 2×10-1 Pa	E = 350 GPa, H = 33 GPa
$Ti_{.19}C_{.81}$	E = 230 GPa, H = 13 GPa
$Ti_{.28}C_{.72}$	E = 280 GPa, H = 22 GPa
$Ti_{.53}C_{.47}$	E = 240 GPa, H = 14 GPa
$Ti_{.90}C_{.10}$	E = 145 GPa, H = 4.5 GPa
440C stainless steel	E = 220 GPa, H = 9 GPa, σy = 4 GPa (FEA)

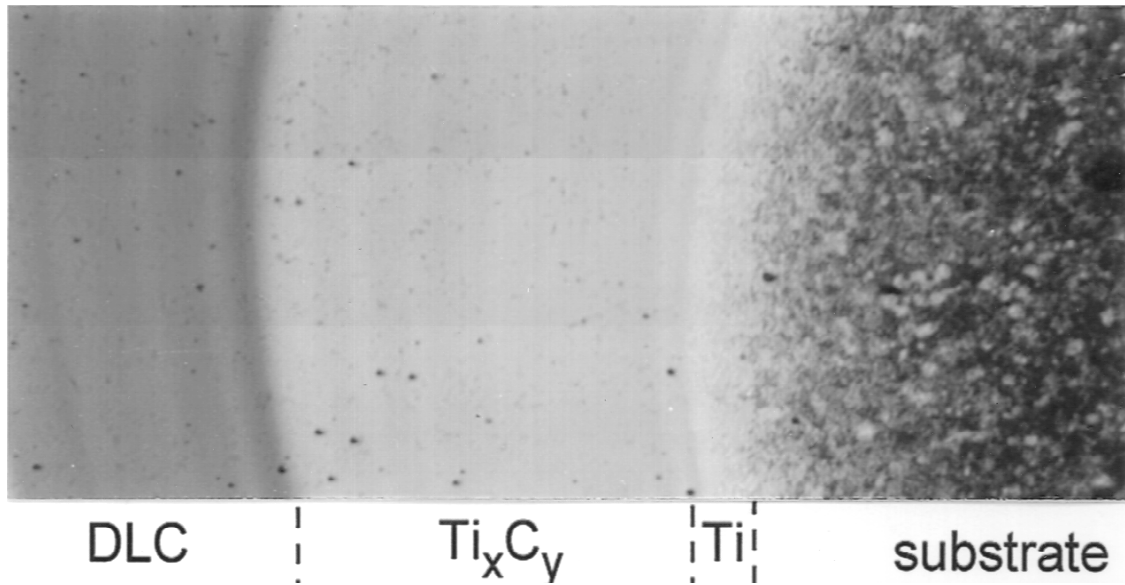Table 1. Mechanical material properties such as modulus of elasticity (E) and hardness (H) for TiC/DLC coating samples

Figure 1. Ti/TiC/DLC functionally gradient coating system that shows the gradual composition variation across the thicknesses of the layers.
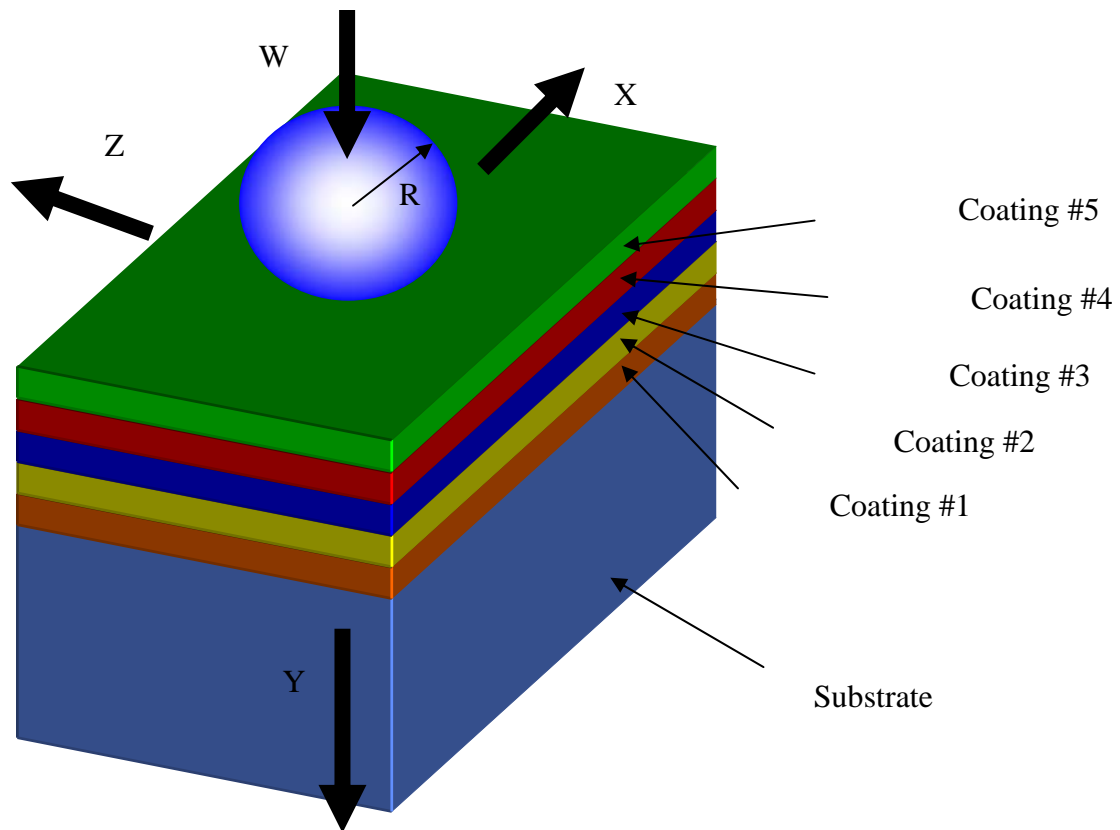
Figure 2. A schematic of point contact for multilayered semi-infinite medium.
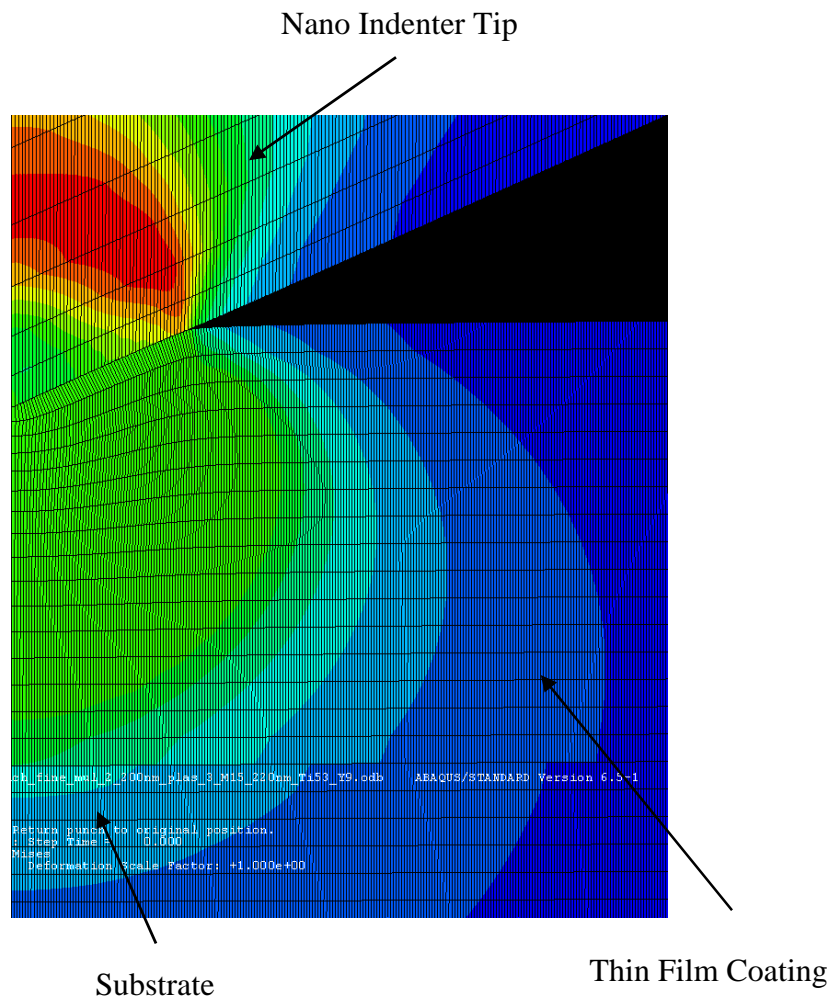
Figure 3. Finite element analysis (FEA) model of the nanoindentation simulation with a conical indenter tip for the coating samples.
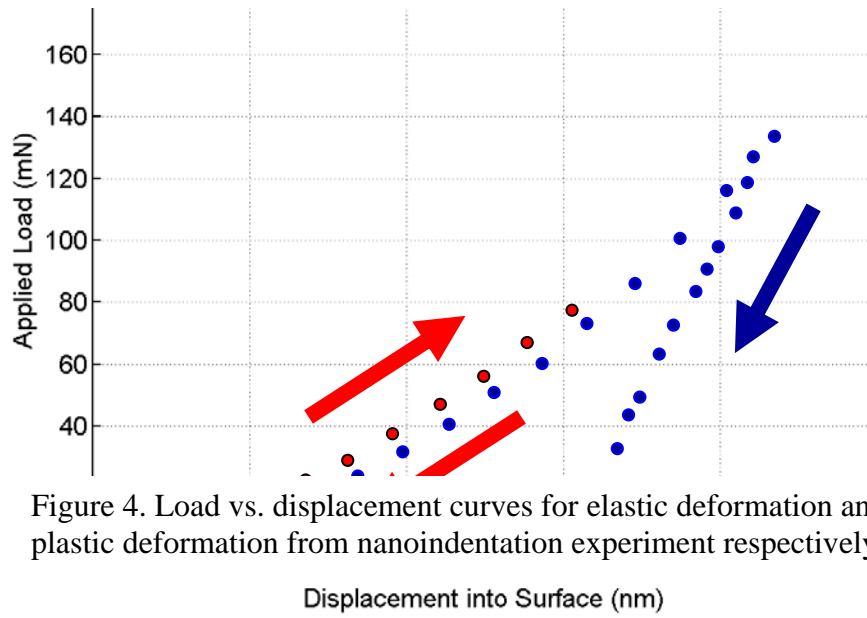
Figure 4. Load vs. displacement curves for elastic deformation and elastic-plastic deformation from nanoindentation experiment respectively.

Legend

• • • • Elastic Deformation

• • • • Elastic Plastic Deformation
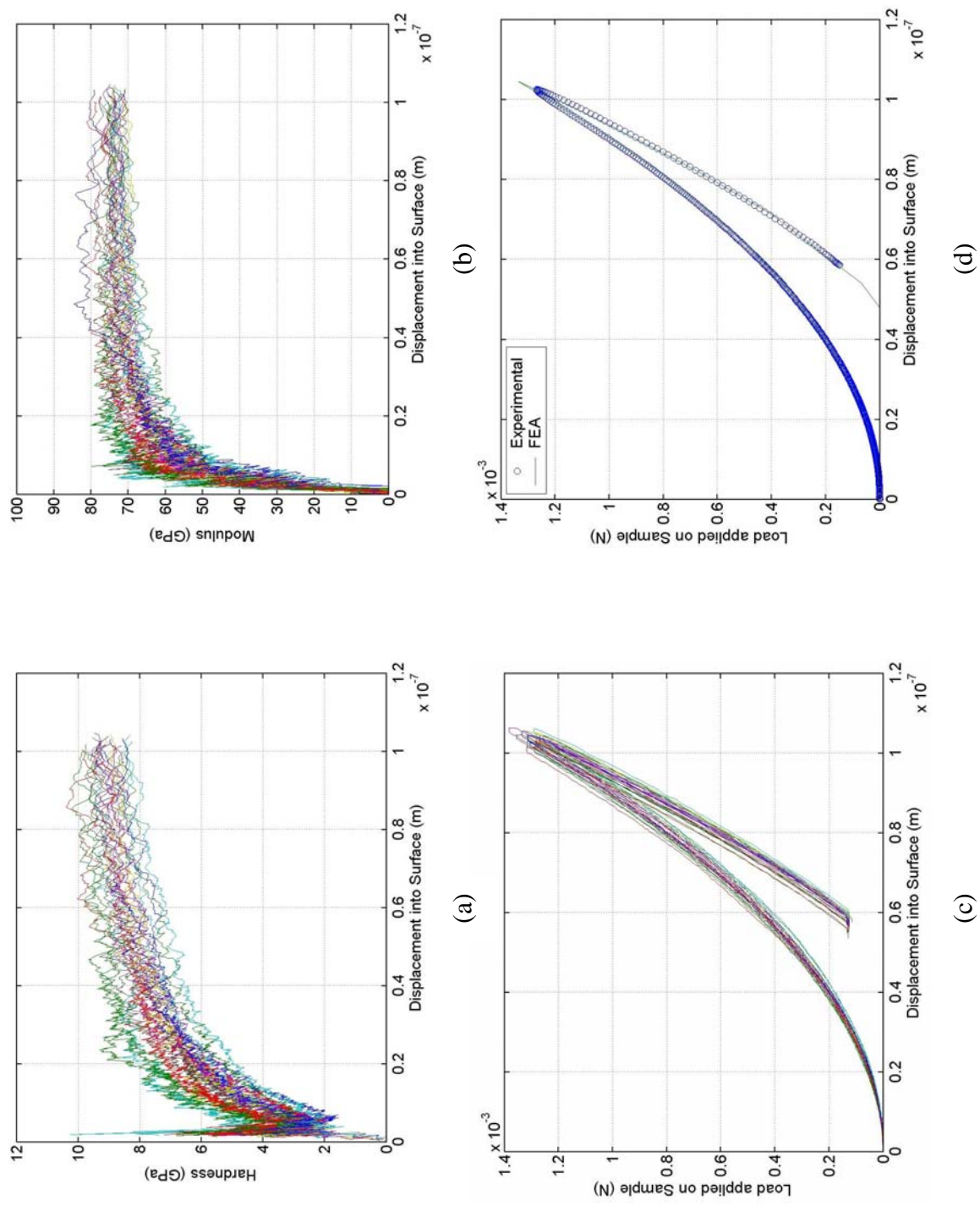
Figure 5.   Nanoindentation results for SiO₂; (a) hardness *vs.* displacement plot, (b) modulus of elasticity *vs.* displacement plot, (c) load *vs.* displacement plot, and (d) load *vs.* displacement plot for experimental results and FEA results.

(a)

(b)
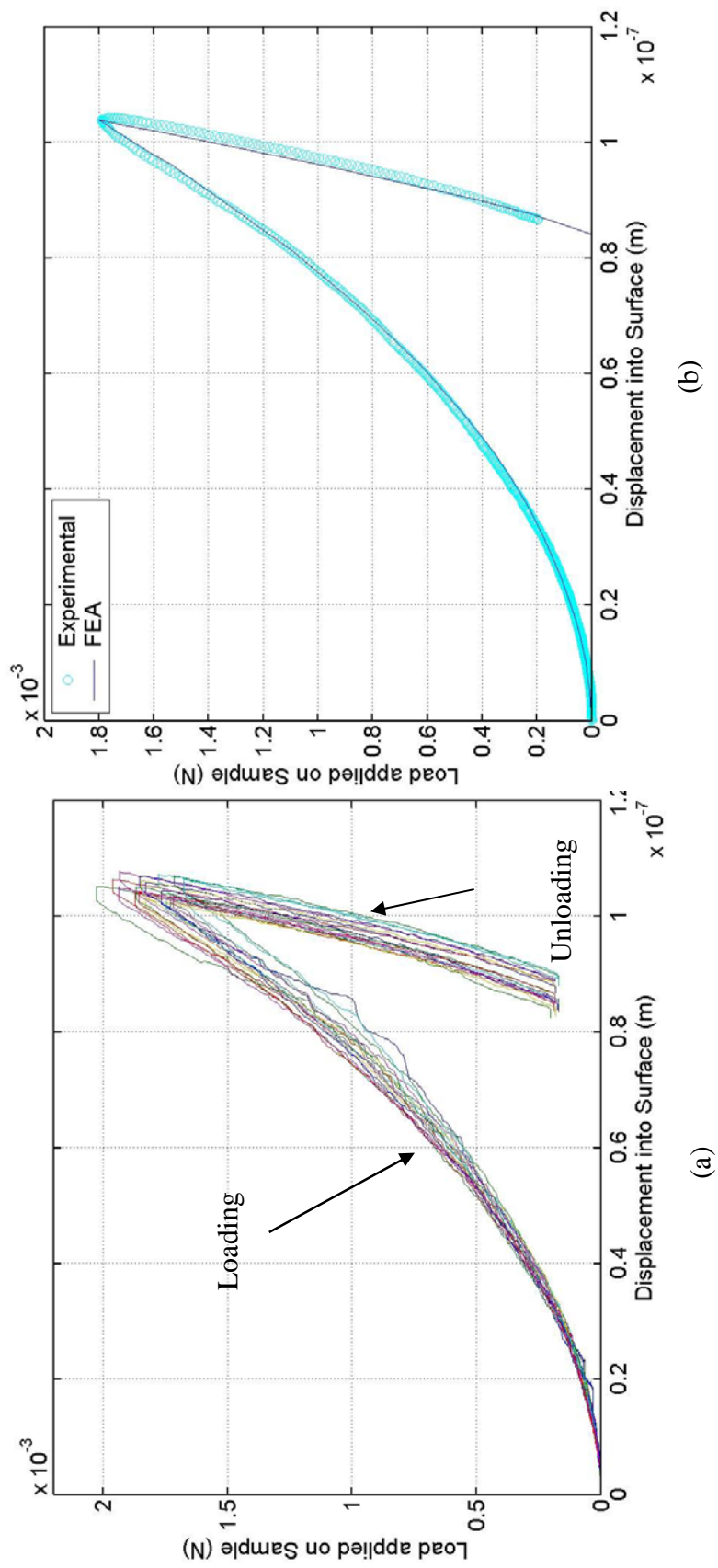
Figure 6.   Nanoindentation results for 440C stainless steel; (a) load *vs.* displacement plot and (b) comparison of load *vs.* displacement plot between average experimental results and best-fit simulation results.

18
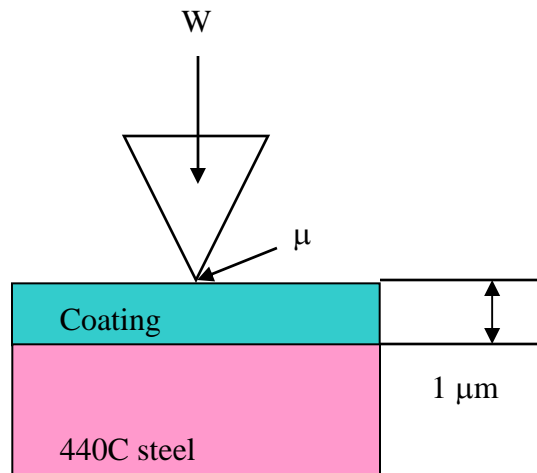
Figure 7. A schematic of nanoindentation with a Berkovich indenter tip on coating samples such as Ti, $Ti_{1-x}C_x$, and DLC on 440C stainless steel to measure the material properties.
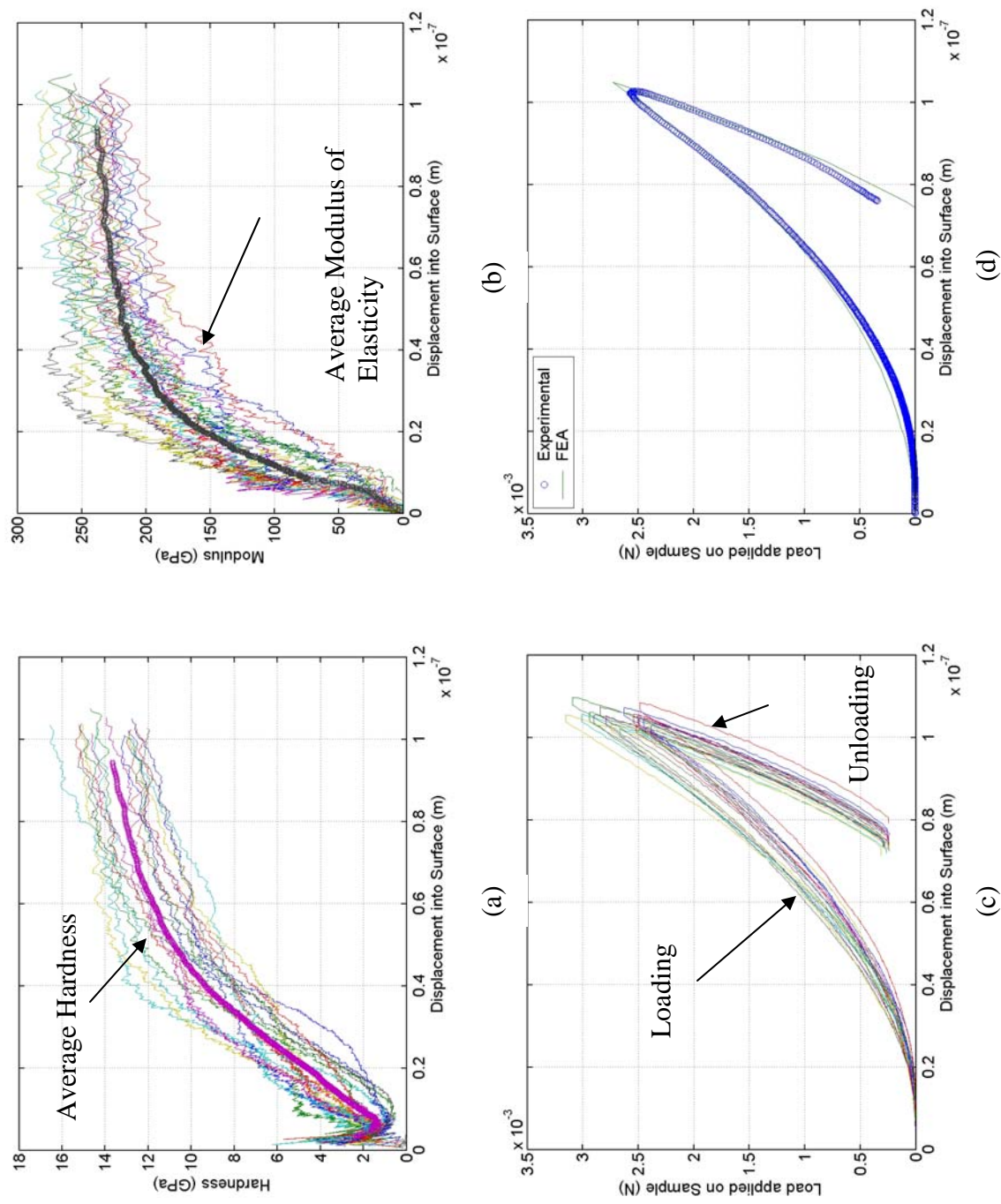
Figure 8.   Nanoindentation results for Ti.$_{53}$C.$_{47}$ coating; (a) hardness *vs.* displacement plot, (b) modulus of elasticity *vs* displacement plot during loading and unloading stages, and (d) comparison of measured average load *vs.* displacement curve and best-fit load *vs.* displacement curve from experiments and FEA simulations, respectively.

Material	Hardness	Elastic Modulus	Yield Strength	Thickness	Poisson's Ratio
DLC at 10^{-5} Pa	70 GPa	650 GPa	45 GPa	400 nm	0.1
DLC at 2×10^{-1} Pa	33 GPa	350 GPa	28 GPa	100 nm	0.1
$Ti_{.10}C_{.90}$	14 GPa	180 GPa	9 GPa	25 nm	0.15
$Ti_{.25}C_{.75}$	21 GPa	260 GPa	14 GPa	25 nm	0.15
$Ti_{.30}C_{.70}$	24 GPa	290 GPa	16 GPa	100 nm	0.20
$Ti_{.50}C_{.50}$	15 GPa	250 GPa	10 GPa	100 nm	0.20
$Ti_{.70}C_{.30}$	11 GPa	200 GPa	7.5 GPa	100 nm	0.25
$Ti_{.90}C_{.10}$	5 GPa	145 GPa	2.5 GPa	50 nm	0.25
α-Ti	2 GPa	136 GPa	1.5 GPa	50 nm	0.25
440C steel	9 GPa	220 GPa	4 GPa		0.30

Figure 9. A schematic of the functionally gradient Ti/TiC/DLC coating design with variation of composition, dimension, and mechanical properties.
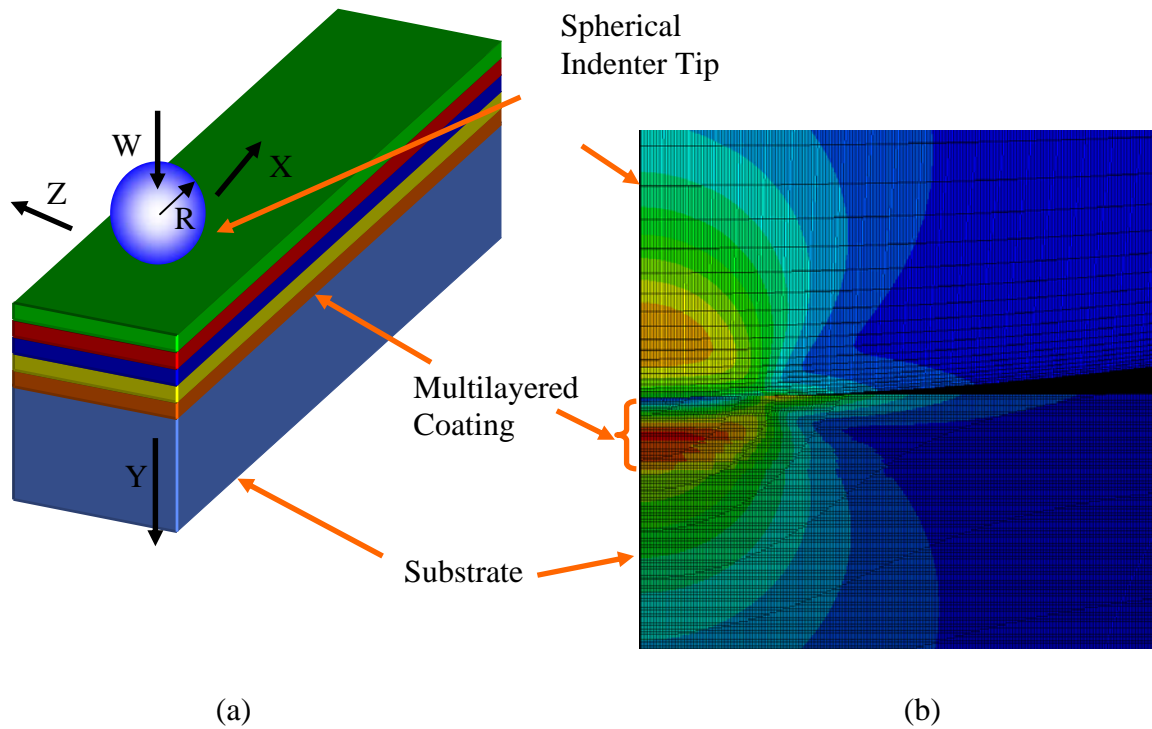
Figure 10. (a) a schematic of nanoindentation on multilayered coating system with a spherical indenter tip, (b)two dimensional axi-symmetric finite element analysis model developed for nanoindentation simulation on a functionally gradient Ti/TiC/DLC multilayered coating system with a spherical indenter tip.
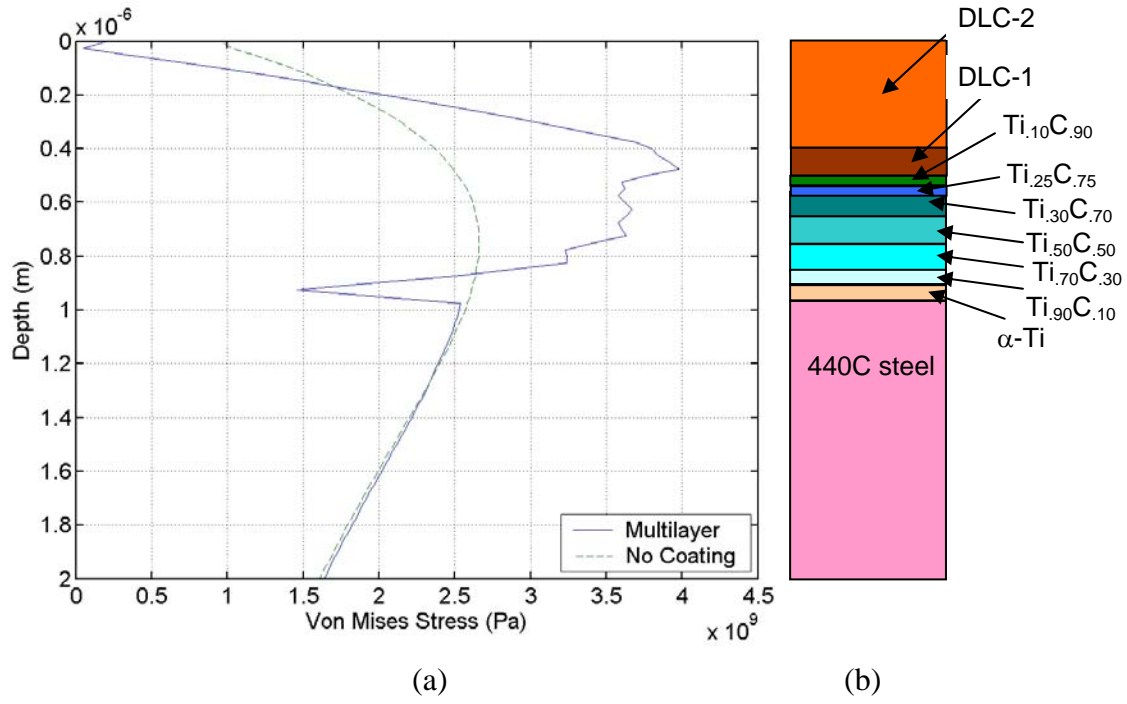
Figure 11. Effect of multilayered FG Ti/TiC/DLC coating system on von Mises stress distribution for the indentation depth, $\delta = 50$ nm, and coefficient of friction, $\mu = 0.0$.
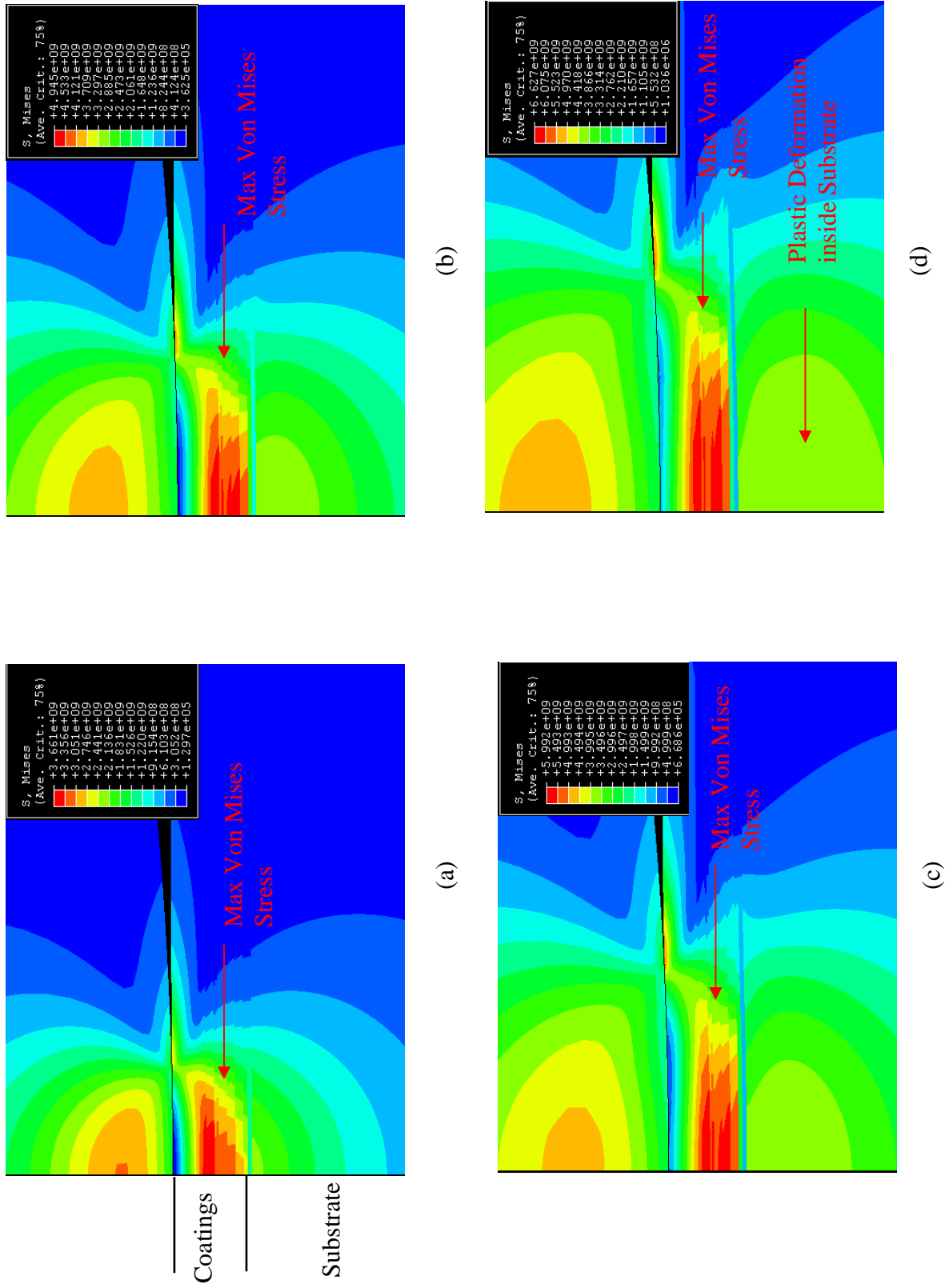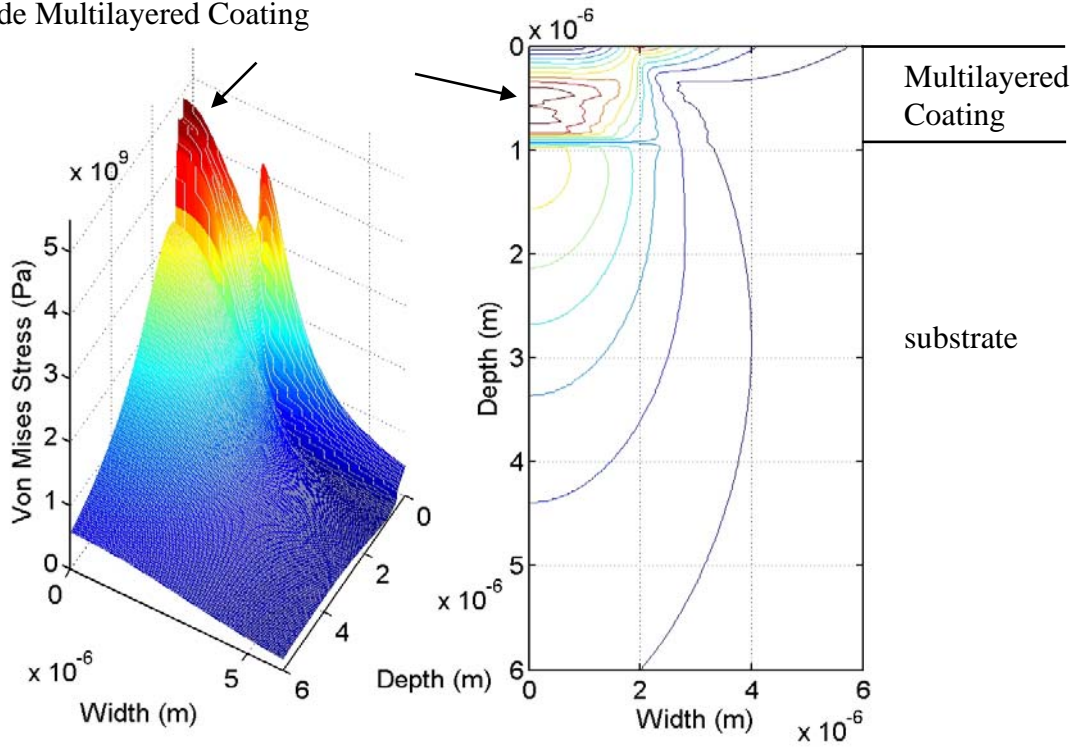
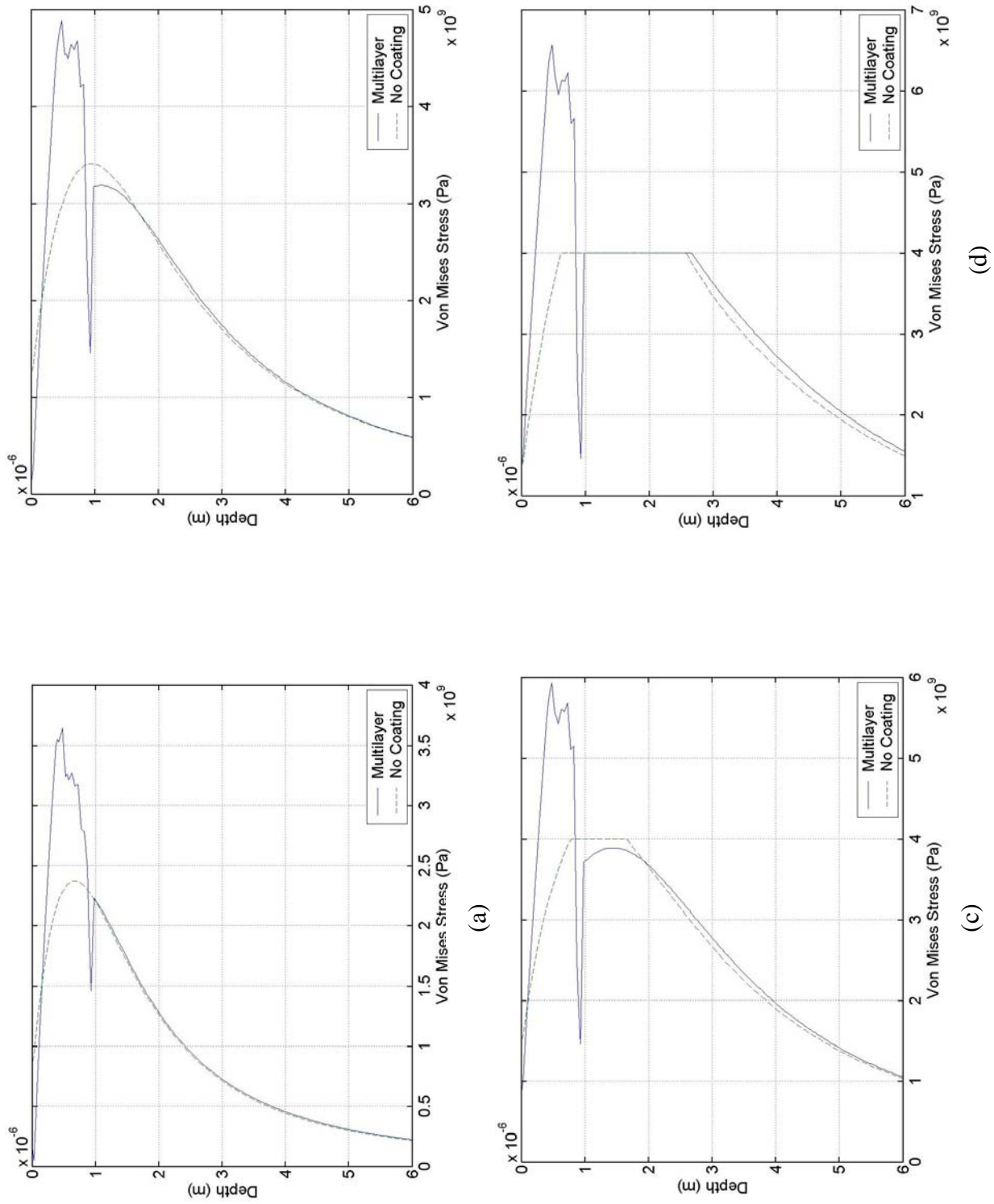Figure 12.   Contour plots of Von Mises stresses distribution generated inside the multilayered FG Ti/TiC/DLC coating system from the FEA model at various indentation depths; (a) δ = 40 nm, (b) δ = 80 nm, (c) δ = 120 nm, and (d) δ = 160 nm.

24

Figure 13. (a) Von Mises stress distribution on the plane of symmetry generated inside the multilayed FG Ti/TiC/DLC coating system for the indentation depth, $\delta = 80$ nm and coefficient of friction, $\mu = 0.0$ and (b) contour plot of Von Mises stress distribution.

Figure 14.   Effect of applied load on Von Mises stresses profiles along the depth direction at the center of the contact at variouis indentation depths for friction coefficient, $\mu = 0.0$; (a) $\delta = 40$ nm, (b) $\delta = 80$ nm, (c) $\delta = 120$ nm, and (d) $\delta = 160$ nm.
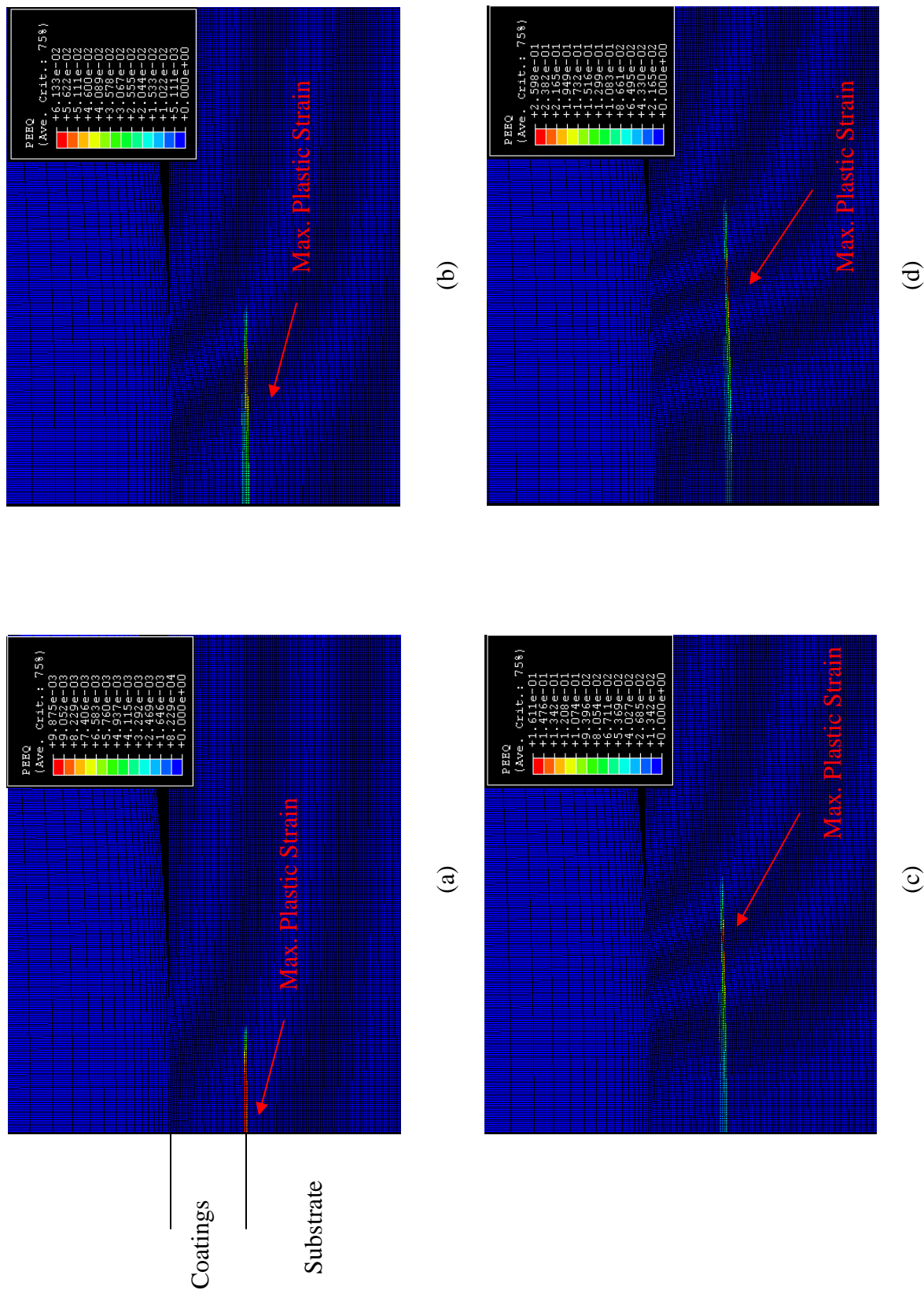
Figure 15. Contour plots of equivalent plastic strain distribution generated on the plane of symmetry inside the multilayered FG Ti/TiC/DLC coating system at various indentation depths; (a) $\delta = 40$ nm, (b) $\delta = 80$ nm, (c) $\delta = 120$ nm, and (d) $\delta = 160$ nm.
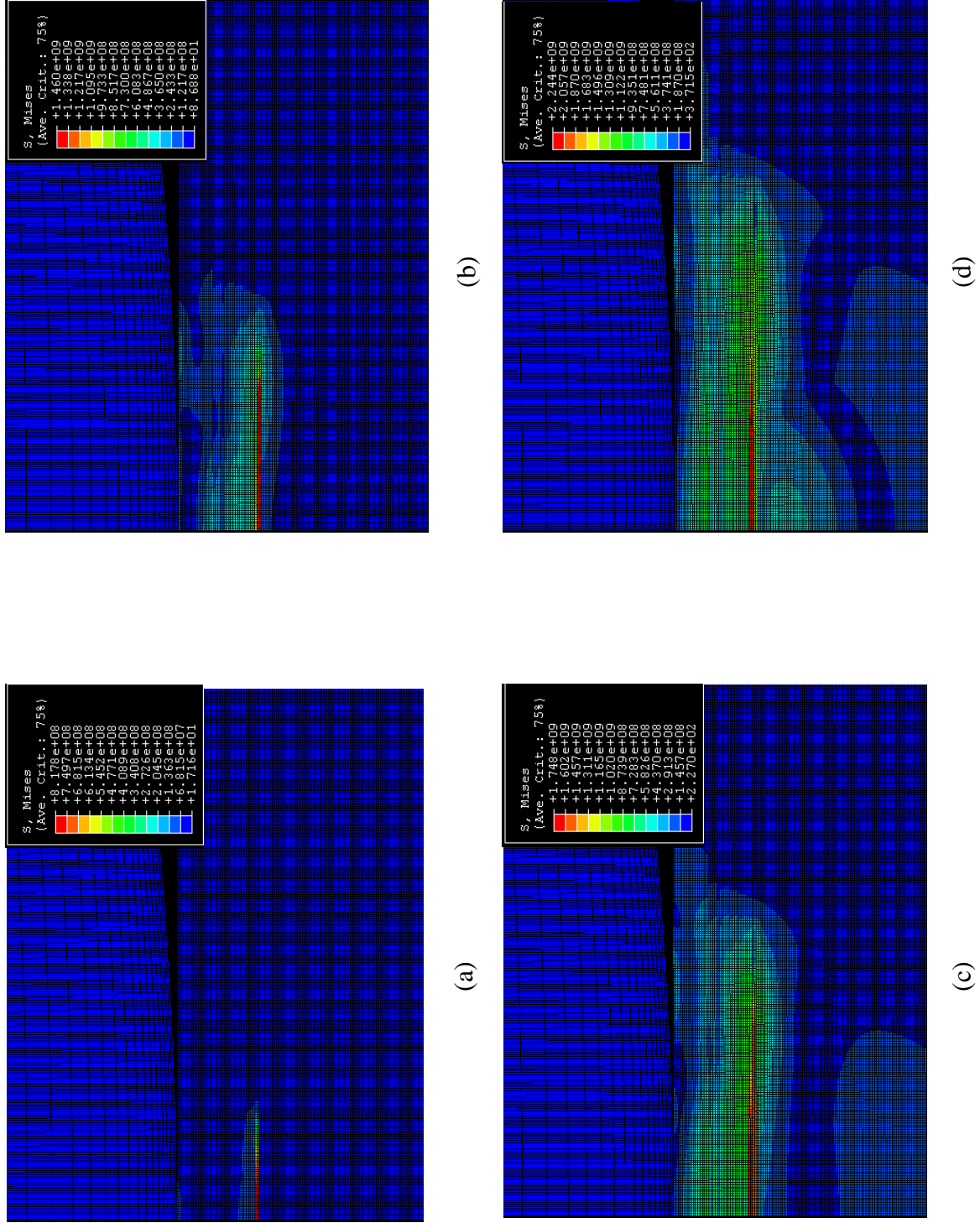
Figure 16. Contour plots of residual von Mises stress distribution generated inside multilayered FG Ti/TiC/DLC coating system after the unloading of nano indenter tip from various indentation depths; (a) δ = 40 nm, (b) δ = 80 nm, (c) δ = 120 nm, and (d) δ = 160 nm.
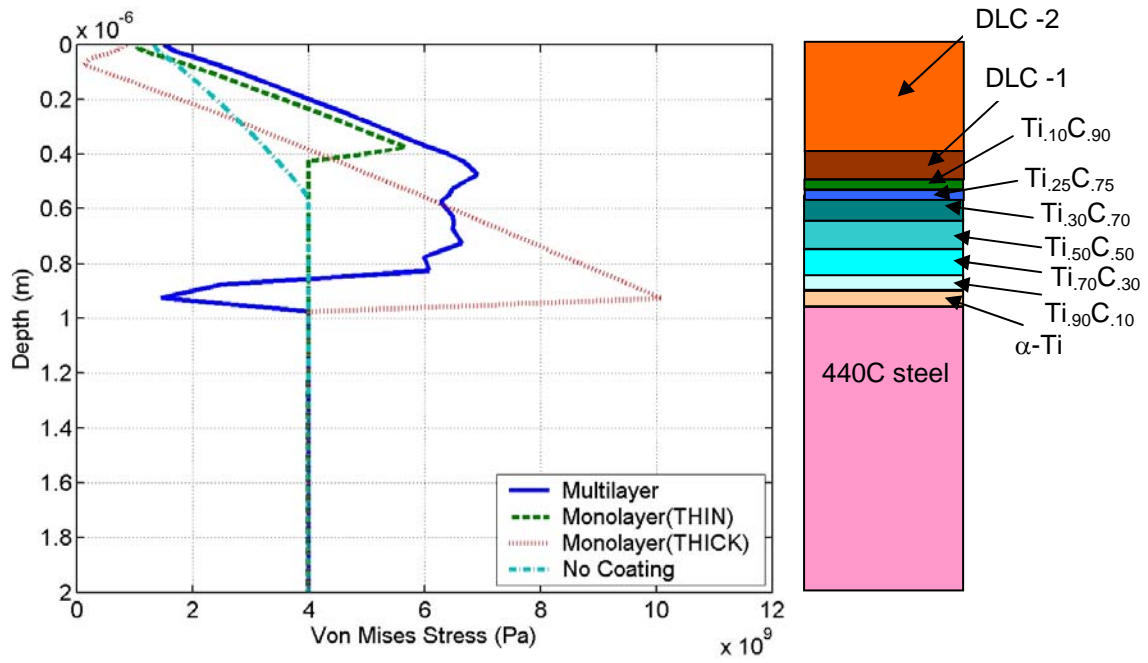
Figure 17. Effect of coating system design on von Mises stress distribution generated inside the coating system for the contact condition, $\delta = 200$ nm and $\mu = 0.0$.